Electronic Supplementary Material (ESI) for Journal of Materials Chemistry A.

Supporting Information

Engineering of Hole-selective Contact for Low Temperature-Processed Carbon Counter Electrode-based Perovskite Solar Cells

Fuguo Zhang,[a] Xichuan Yang,[a,c] Ming Cheng,[b] Jiajia Li,[a] Weihan Wang,[a] Haoxin Wang[a] and Licheng Sun[a,b]*

Experimental

Reagents & Materials

All chemicals, reagents, and solvents were purchased from commercial sources such as Sigma-Aldrich, Alfa, and TCI and used as received without any purification unless otherwise specified. All reactions were performed under inert atmosphere.

Synthesis of CH_3NH_3I

The CH_3NH_3I was synthesized by reacting 24 ml of CH_3NH_2 and 10 ml of HI in a 250 ml round bottom flask at 0 °C for 2 h with continuous stirring. The resulting solution was evaporated at 50 °C for 1 h and produced synthesized chemicals (CH_3NH_3I). The precipitate was redessolved in ethanol and recrystallized from diethyl ether, the precipitate was then filtered and washed three times with diethyl ether and dried at 60 °C under vacuum for 24 h to afford the desired pure CH_3NH_3I as white crystals.

Synthesis of TPDI (*5,10,15-triphenyl-5H-diindolo[3,2-a:3',2'-c]carbazole****)***

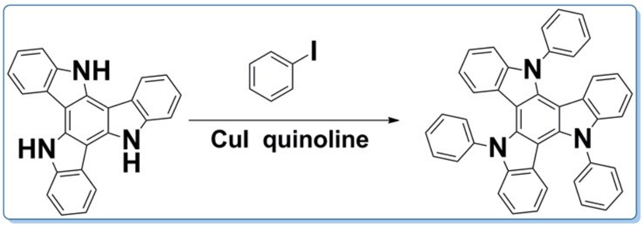

Scheme S1. The synthetic route of TPDI.

The TPDI was synthesized by adaption of relevant literature procedure as described in reference 23 and the synthetic route was shown in Scheme S1. To be specified, to a solution of triazatruxene (1.00g, 2.90 mmol), iodobenzene (4 g, 19.66 mmol) in 50 mL of quinoline, CuI (2.20 g, 11.56 mmol) and K_2CO_3 (1.60 g, 11.50 mmol) under nitrogen were added. After stirring at 180 ºC for 2.5 days under a N_2 atmosphere, the reaction mixture was allowed to cool to room temperature and subsequently diluted with dichloromethane (120 mL) followed by filtering through a plug of celite. The resulting filter cake was further washed with dichloromethane (100 mL). The filtrate was concentrated in a vacuum. The residue was purified by column chromatography eluting with 1/4 to 1/1 dichloromethane–hexane to give a pale yellow solid of the desired product. Finally, the obtained solid was re-crystallized in a mixed solution of dichloromethane and methanol to provide a white solid of the product TPDI in 80% yield. ^{1}H NMR (500 MHz, DMSO) δ 7.79 – 7.65 (m, 15H), 7.26 (t, J = 13.4 Hz, 3H), 7.19 (t, J = 7.6 Hz, 3H), 6.73 (t, J = 7.5 Hz, 3H), 5.99 (d, J = 8.1 Hz, 3H). ^{13}C NMR (126 MHz, DMSO): 136.40, 135.73, 132.45, 124.73, 124.52, 123.96, 123.77, 122.99, 117.93, 117.29, 114.75, 113.68, 104.62, 99.18. MS: *m/z*:573.2197 [M^+].

Characterization of TPDI.

^{1}H NMR and ^{13}C NMR spectra were recorded on a Varian Mercury 400 spectrometer. Chemical shifts were calibrated against TMS as an internal standard. Cyclic voltammetry measurement was carried out with CHI 630 Electrochemistry Workstation. Redox potential of material was measured in chloroform solution with 0.1 M $(n\text{-}C_4H_9)_4NPF_6$ as the supporting electrolyte. A glassy carbon electrode with a surface area of 0.785 cm^2 was used as working electrode. The counter electrode consisted of a platinum wire and the reference electrode was an $Ag/AgNO_3$ electrode. The redox potential was calibrated against Fc/Fc^+ as an internal standard. Thermogravimetrical analysis (TGA) was performed on TA Q500 thermo gravimetric apparatus (TA Instruments, USA) at a heating rate of 10 ºC/min under nitrogen atmosphere. Differential scanning calorimetry (DSC) was conducted on TA Q20 Instrument (TA Instruments, USA) at a heating rate of 10 ºC /min under nitrogen atmosphere.

Preparation of mesoporous TiO_2 film

Perovskite thin film and solar cells were fabricated on FTO-glass substrate with a sheet resistance of 14 Ω sq^{-1}. Fluorine–doped tin oxide coated glass (Pilkington TEC 15) was firstly patterned by etching with Zn powder and 2 M HCl. The etched substrate was then cleaned with surfactant and rinsed with acetone and ethanol and de-ionized water and finally treated under oxygen plasma for 30 min to remove the last traces of organic residues.

A thin layer of compact anatase TiO_2 of roughly 30-40 nm in thickness was formed through spin-coating of titanium diisopropoxide bis(acetylacetonate) diluted in anhydrous ethanol at a volumetric ratio of 1:20 at 2000 r.p.m. for 60s and consequently heating at 500 °C for 30min. Mesoporous TiO_2 layers were deposited by spin–coating TiO_2 paste (Dyesol 18NR–T) diluted in anhydrous ethanol at ratio of 1:4 by weight at 2000 r.p.m. for 60s and consequently heating at 500 °C for 30min. The as prepared nanoporous TiO_2 films were then dipped into a 40 mM $TiCl_4$ aqueous solution for 30 min at 70 °C, dried at ambient atmosphere and then sintered at 500 °C for 30min.

Device fabrication

The prepared mesoporous TiO_2 films were preheated to ~90 °C, and then infiltrated with a solution of PbI_2 in *N, N'*-dimethylformamide (1.3 M, 600 $mg.mL^{-1}$) by spin coating at 2500 r.p.m. for 30s and dried at 100 °C for 15 min immediatelly. After cooling to room temperature, dipping the resulted TiO_2/PbI_2 composite film into a solution of CH_3NH_3I in 2-isopropanol (10 $mg.mL^{-1}$) for 60 min. The resulting perovskite film was washed with dry 2-propanol for ~ 20s to remove the residue CH_3NH_3I on surface of perovskite film and followed by spin-coating with N_2 flow, dried at 100 °C for 30 min.

The HTMs were coating via solution process by following details. Spiro-OMeTAD/chlorobenzene (72.3 $mg.ml^{-1}$) solutions with or without additives containing 17.5 μL Li-TFSI/acetonitrile (520 $mg.mL^{-1}$) and 28.8 μL TBP were spin-coated on substrate of $CH_3NH_3PbI_3$/mp-TiO_2/bl-TiO_2/FTO at 2000 r.p.m. for 40 s, respectively. Under the same molar concentration, doping conditions, and spin-coating methods with spiro-OMeTAD, TPDI/chlorobenzene (34 mg/ml) with or without additives were deposited on $CH_3NH_3PbI_3$/mp-TiO_2/bl-TiO_2/FTO substrate. Finally, the low temperature processed commercial carbon paste (CC, Shenzhen DongDaLai Chemical Co., Ltd.) was deposited on the prepared film with a fixed active area of 0.12-0.16 cm^2 by doctor–blading technique, and dried at 100 °C for 30 min. All these procedures were carried out on naturally ambient atmosphere. The hole-only device for hole mobility measurements consists of ITO/PEDOT:PSS (~30nm) / TPDI (~150nm)/ MoO_3 (~20nm)/ Al (~100nm). TPDI (34 mg) was dissolved in 1 ml chlorobenzene and stirred for 30 min. The Pre-cleaned ITO substrate was treated with UV-ozone for 25 min, and then a ~30 nm PEDOT: PSS layer was spin-coated onto the ITO substrate from an aqueous solution (Baytron PVP AI 4083), followed by baking in an oven at 150 °C for 10 min. the active layer was obtained by spin-coating the TPDI solution at 2000rpm for 30 s. The active layer thickness is certified by HR-SEM to be ~150 nm. A bilayer cathode structure of MoO_3 (~20 nm)/ Al (~100 nm) was thermally evaporated on top of the active layer.

Characterizations

The UV-vis spectra of perovskite and TPDI were obtained by using an Agilent 8453 spectrophotometer. Steady-state and transient photoluminescence spectra were obtained with a LP920 laser flash spectrometer (Edinburgh Instruments). The pump pulse is provided by a nanosecond tunable OPOlett-355Ⅱ laser. The photocurrent–voltage (*J–V*) characteristics of the solar cells were measured using a Keithley 2400 Source-measure unit under illumination of a simulated sunlight (AM 1.5G, 100 $mW \cdot cm^{-2}$) provided by an Oriel Sol3A solar simulator (Newport USA, Model: 94023A) with an AM 1.5 filter in ambient air. Light intensity was calibrated with a Newport calibrated standard Si reference cell (SER. No: 506/0358). A black mask with a circular aperture (0.09 cm^2) smaller than the active area of the square solar cell (0.12-0.16 cm^2) was applied on top of the cell. The *J-V* curves were obtained in air through reverse (1.2 V— -0.5 V) scanning at the rate of 20 mV S^{-1}. For the measurements of hysteresis, the *J-V* curves were obtained in air through reverse (1.2 V-0 V) or forward scan (0

V-1.2V) at the rate of 20mV S^{-1}. The measurement of the incident photo–to–current conversion efficiency (IPCE) was obtained by a Hypermono−light (SM−25, Jasco Co. Ltd., Japan).

X−ray diffraction and extra high resolution scanning electron microscopy.

X−ray powder diffraction measurements were performed in grazing incidence X−ray diffraction (GIXRD) mode on the D8 Advance diffractometer (Bruker AXS, Karlsruhe, Germany). XRD patterns within the range 10° to 70° 2θ were recorded at room temperature using Cu Kα radiation with the following measurement conditions: tube voltage of 40 kV, tube current of 40 mA, step-scan mode with a step size of 0.02° 2θ and counting time of 1 s per step. The value of the grazing incidence angle was 2.5°. HR–SEM was performed with FEI (Field Emission Instruments: Nova Nano SEM 450), The USA.

EIS (electrochemical impedance spectroscopy) measurements

The electrochemical impedance measurements were carried out at different applied bias under one sun light illuminating condition using an impedance/gain–phase analyzer (Zahner Model: Zennium, Serial No: 40037, German) electrochemical workstation with the frequency range from 10 mHz to 1 MHz. The magnitude of the alternative signal was 10 mV.

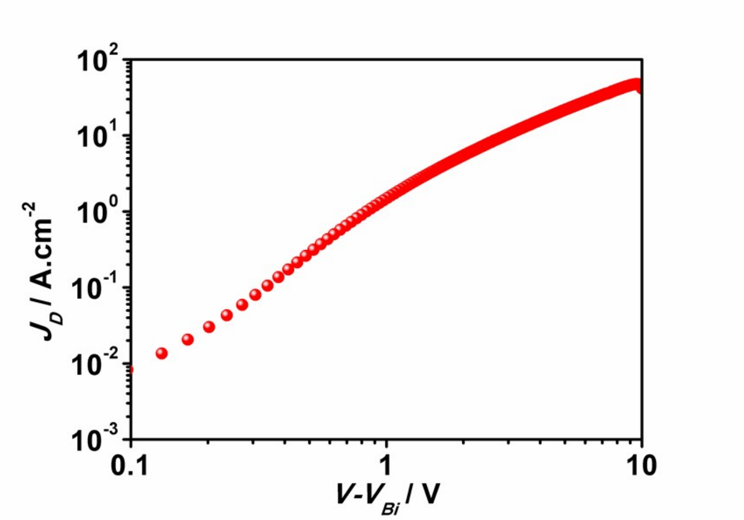

Figure S1. J-V characteristics of the TPDI based hole-only device.

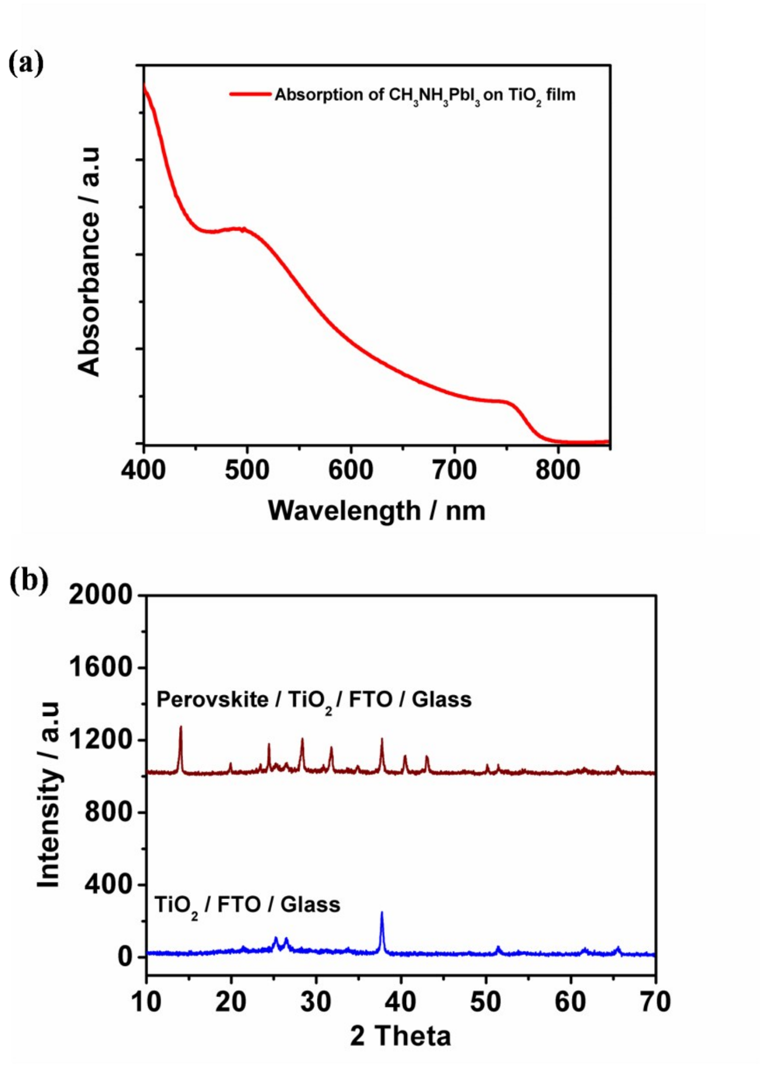

Figure S2. (a) UV-vis absorption of $CH_3NH_3PbI_3$ film on mp-TiO_2 film. (b) X-ray diffraction patterns of mp-TiO_2 on FTO substrate (blue line) and $CH_3NH_3PbI_3$ on mp-TiO_2 film (brown line).

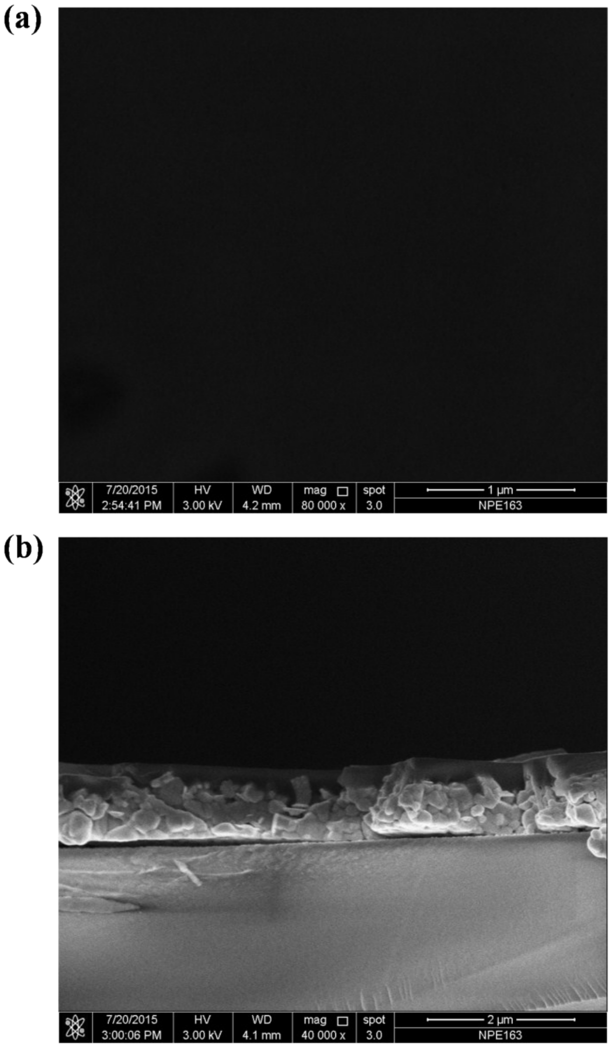

Figure S3. HR-SEM images of (a) top view and (b) cross sectional view of TPDI/$CH_3NH_3PbI_3$/Galss film.

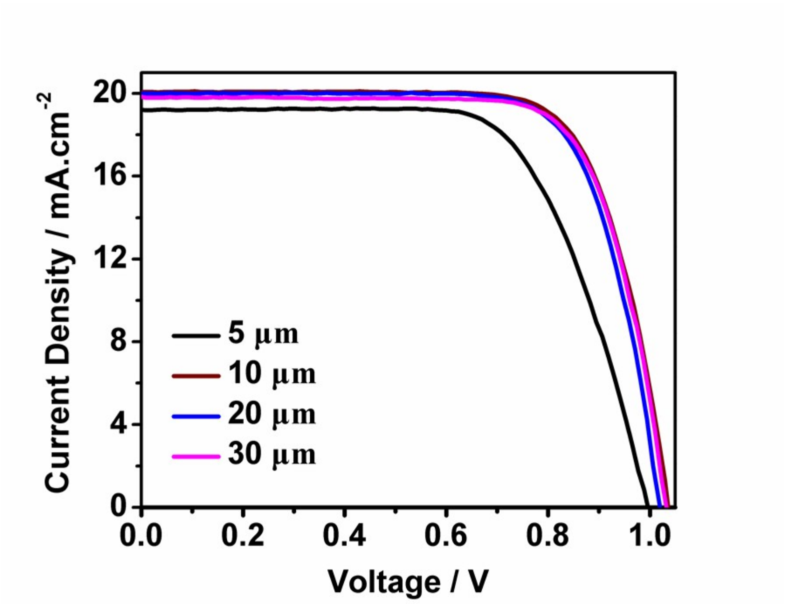

Figure S4. The photocurrent density-photovoltage (*J-V*) characteristic of the Glass/FTO/Compact TiO_2/Mesoporous-TiO_2/$CH_3NH_3PbI_3$/TPDI(doped)/Carbon structured perovskite solar cell based on different thickness of carbon counter electrodes.

Table S1. Photovoltaic characteristics of perovskite solar cells with different thickness of carbon counter electrode.

Carbon thickness	Sheet (square) resistance	J_{sc} / mA.cm^{-2}	V_{oc} / V	*FF* / %	PCE / %
5 µm	17.56 Ω/□	19.2	0.99	67.3	12.8
10 µm	6.34 Ω/□	20.1	1.03	73.7	15.3
20 µm	4.51 Ω/□	20.1	1.02	73.9	15.2
30 µm	2.36 Ω/□	19.9	1.03	74.2	15.2

In our study, the conductivity of this kind of commercial carbon is very good, the thickness of the carbon affects its sheet (square) resistance. Therefore, in order to understand the exact influence of different thickness of carbon CE on the photovoltaic performances. Devices with different thickness of carbon as counter elecreode were fabricated and the corresponding photovoltaic performance were also recorded.

The doped-TPDI was used as hole transport material. The solar cell devices were fabricated with structure of Glass/FTO/Compact TiO_2/Mesoporous TiO_2/$CH_3NH_3PbI_3$/TPDI(doped)/Carbon. Four-point probe measurement was deployed to investigate the conductivity of the as-prepared carbon counter electrodes with different film thickness. As illustrated in **Table S1**, we found that the sheet resistance of the carbon films decreases as the carbon film thickness increase. To be specific, the 5 µm thick carbon film produced a large sheet resistance of 17.56 Ω/□, increasing the carbon film thickness to 10µm, 20µm and 30µm, the sheet resistance decreased to 6.34 Ω/□, 4.51 Ω/□ and 2.36 Ω/□, respectively. Detailed device parameters corresponding to different carbon thicknesses were summarized in **Figure S4** and **Table S1**, from which we found that the 5µm thick carbon CE showed a V_{oc} of 0.99 V, J_{sc} of 19.2 mA.cm^{-2}, and a *FF* of 67.3%, corresponding to a PCE of 12.8%, while the 10 µm thick carbon CE afforded an enhanced V_{oc} of 1.03 V, J_{sc} of 20.1 mA.cm^{-2}, *FF* of 73.7%, thus yielded a improved PCE of 15.3%. Further increase the thickness of the carbon CE thickness to 20 µm and 30 µm did not significantly enhance the performance of the corresponding perovskite solar cells and identical parameters were obtained. The inferior performance of 5 µm thick carbon CE based device (especially for *FF*) should be ascribed to the poor conductivity of thin carbon film, which limit the hole collection and transportation to some extent. Although better conductivity of the CEs were achieved as the film thickness increased from 10μm to 20μm or even thicker 30μm, the J_{sc} and V_{oc} kept almost unchanged and slightly larger *FF* were demonstrated. The results demonstrated that the conductivity of 10μm thick carbon CEs is good enough for charge extraction and transportation.

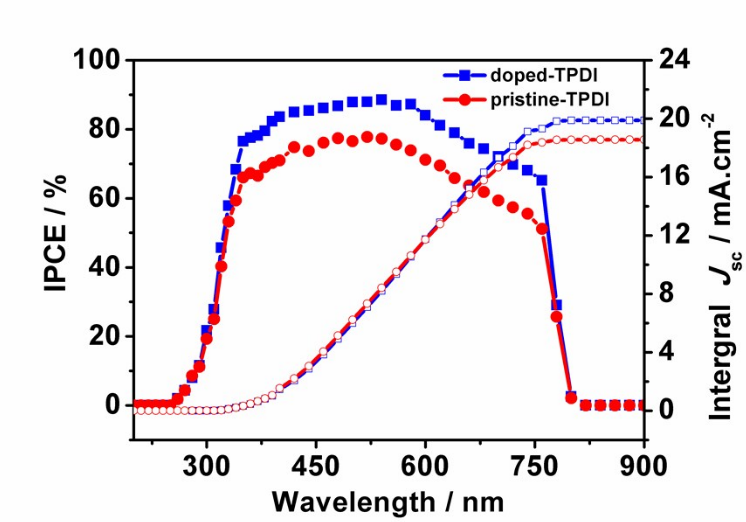

Figure S5. Incident photon-to-electron conversion efficiency (IPCE) spectra and the corresponding integrated photocurrent density J_{sc} for the doped-TPDI (blue) and pristine-TPDI (red) based PSCs. Integrated J_{sc} was calculated to be 19.9 mA·cm^{-2} and 18.6 mA·cm^{-2}, respectively for these two kinds of devices. Aperture cell area was 0.09 cm^2.

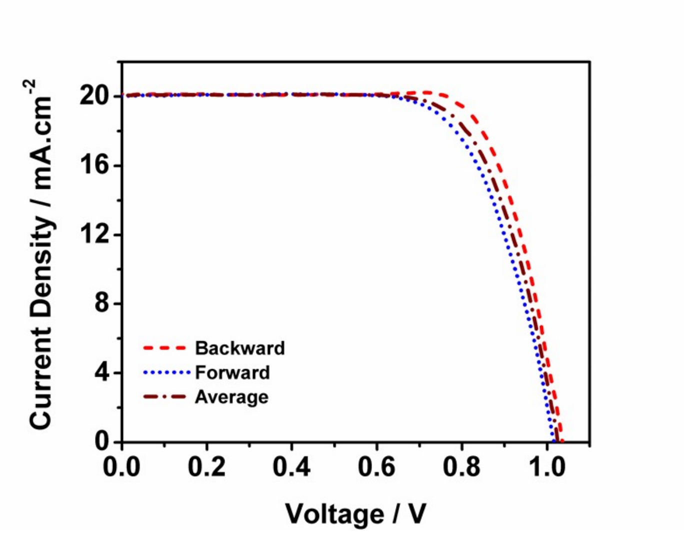

Figure S6. *J-V* curves of representative perovskite/doped TPDI/carbon based device under different scan directions.

Table S2. Summary of photovoltaic performances of the solar cells with TPDI as HTM, evaluated under AM 1.5 G irradiation with different scan directions.

Scanning direction	J_{sc} [mA·cm^{-2}]	V_{oc} [V]	*FF* [%]	*PCE* [%]
Forward	20.1	1.02	69.5	14.1
Reverse	20.1	1.03	74.9	15.5
Average	20.1	1.03	72.2	14.8

Table S3. Photovoltaic parameters of a batch of ten devices with doped TPDI as HTM measured under AM 1.5 G (100 mW.cm^{-2}) illuminations

Devices	V_{oc} [V]	J_{sc} [mA·cm^{-2}]	*FF* [%]	PCE [%]
1	1.01	19.9	70.7	14.3
2	1.02	20.1	74.2	15.2
3	1.04	19.8	72.8	14.9
4	1.01	20.2	69.8	14.3
5	1.02	20.5	69.4	14.5
6	1.03	20.0	73.8	15.1
7	1.03	20.1	75.3	15.5
8	1.02	20.1	70.0	14.4
9	1.02	20.1	73.1	15.0
10	1.02	20.0	69.1	14.0
Aver. ± std dev (%)	1.02±0.01	20.1±0.19	71.8±2.3	14.7±0.49

Table S4. Photovoltaic parameters of a batch of ten devices with pristine TPDI as HTM measured under AM 1.5 G (100 mW·cm^{-2}) illuminations.

Devices	V_{oc} [V]	J_{sc} [mA·cm^{-2}]	*FF* [%]	PCE [%]
1	1.02	18.2	71.7	13.3
2	1.01	18.6	68.8	12.8
3	1.02	18.7	70.2	13.4
4	1.01	18.0	69.2	12.6
5	1.01	18.1	70.6	12.9
6	1.03	18.6	69.2	13.2
7	1.02	18.1	68.3	12.6
8	1.01	19.0	67.6	12.9
9	1.02	18.8	66.5	12.7
10	1.01	18.4	71.3	13.3
Aver. ± std dev (%)	1.02±0.01	18.4±0.34	69.7±1.6	13.0±0.29

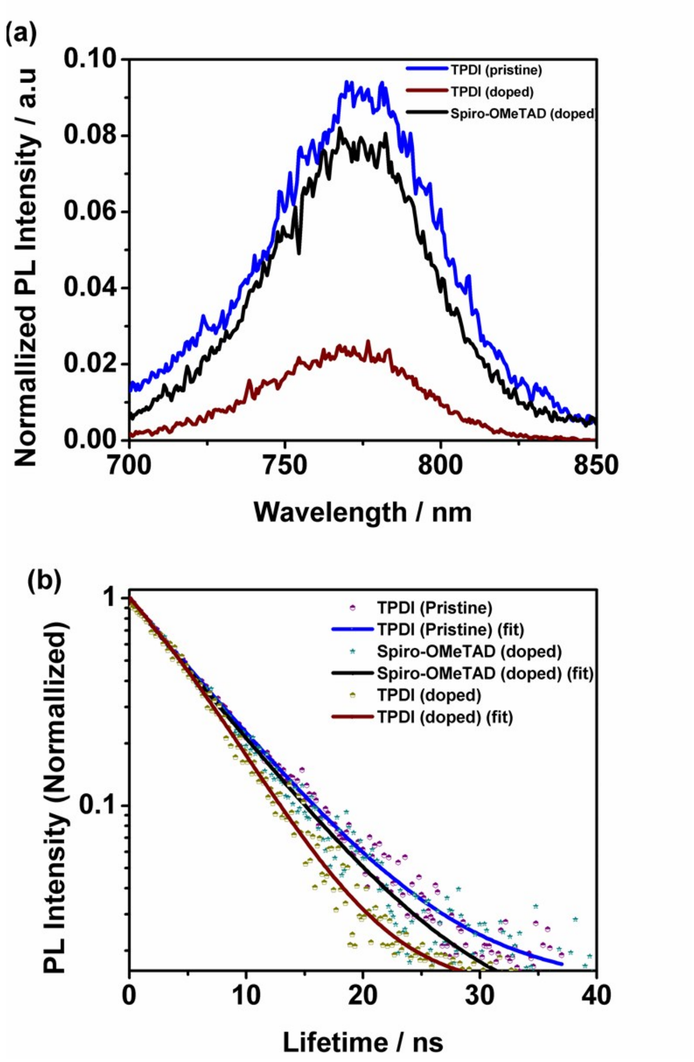

Figure S7. (a) Steady-state PL spectra and (b) time-resolved PL decay transient spectra of different *p*-type quenchers of perovskite film.

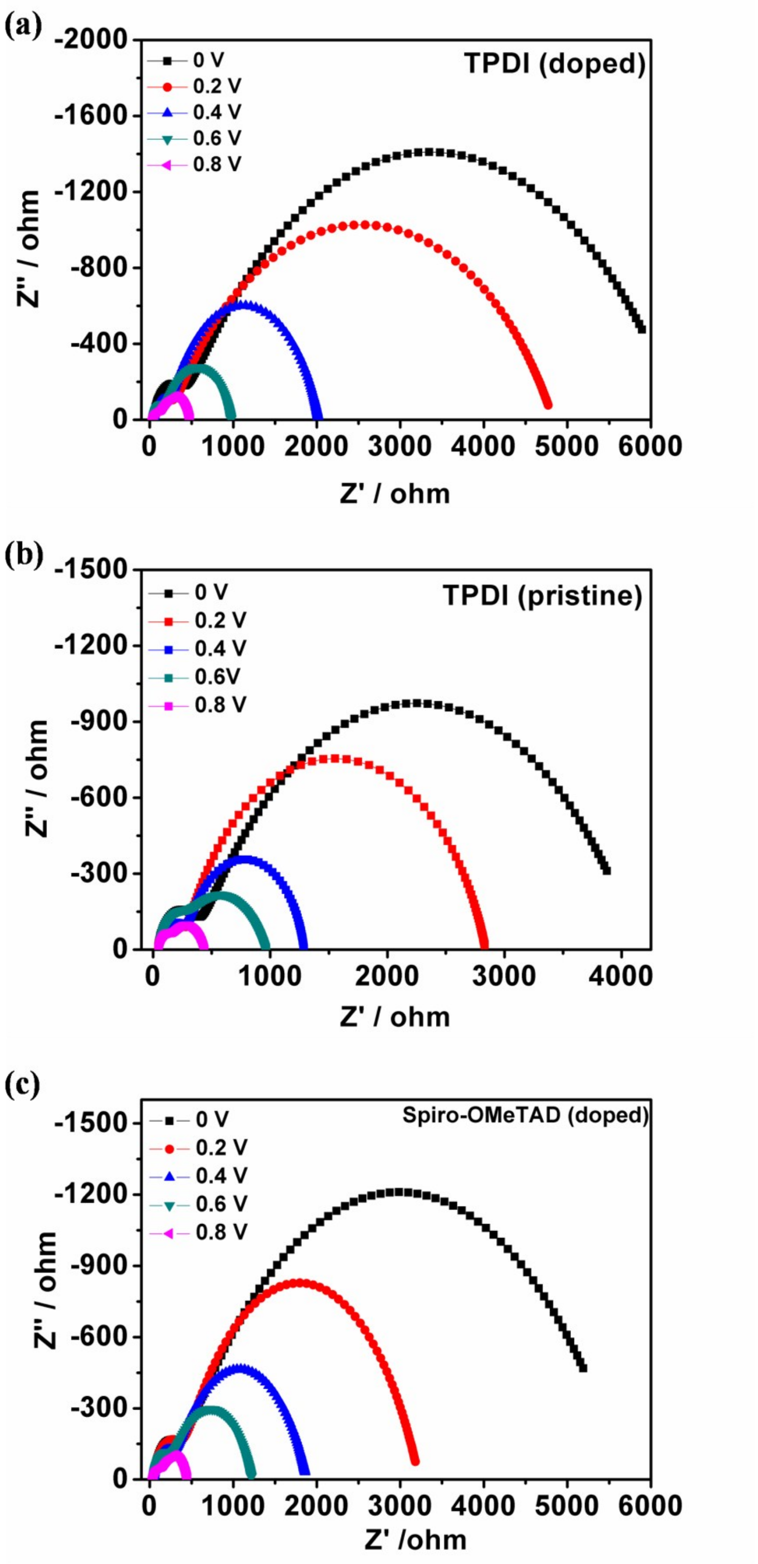

Figure S8. Bias dependence of Nyquist plots of devices with (a) doped TPDI, (b) pristine TPDI and (c) doped spiro-OMeTAD

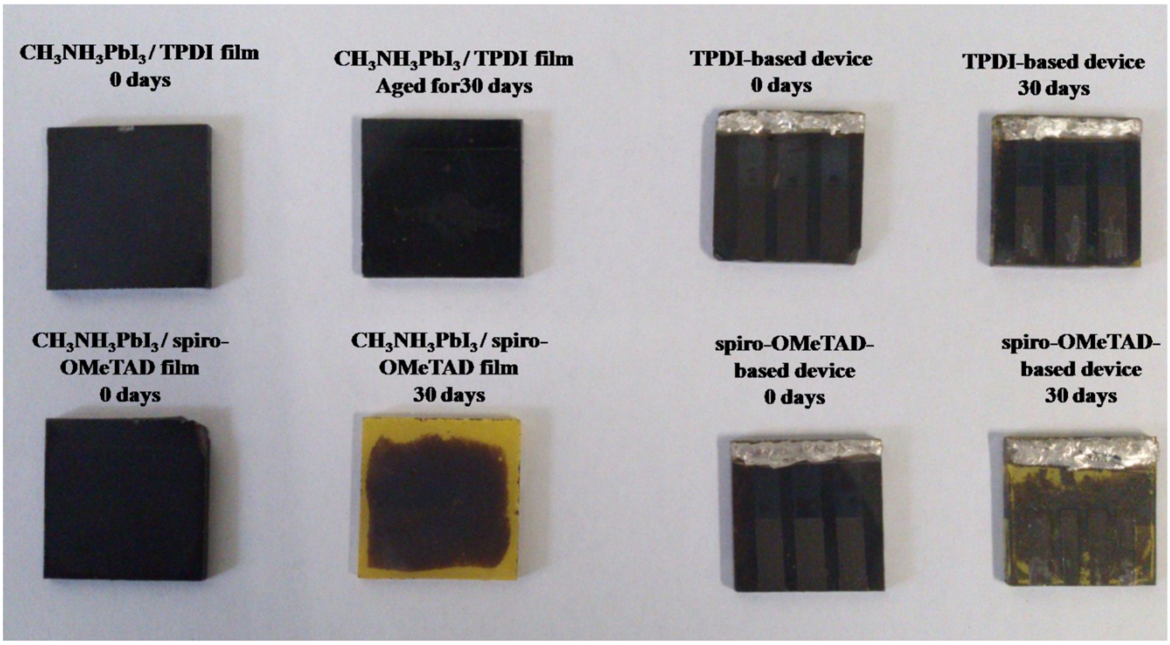

Figure S9. The photograph of the fresh $CH_3NH_3PbI_3$/HTM films and the films after storage in ambient atmosphere for 30 days. And the corresponding phototographs of different HTMs based devices.

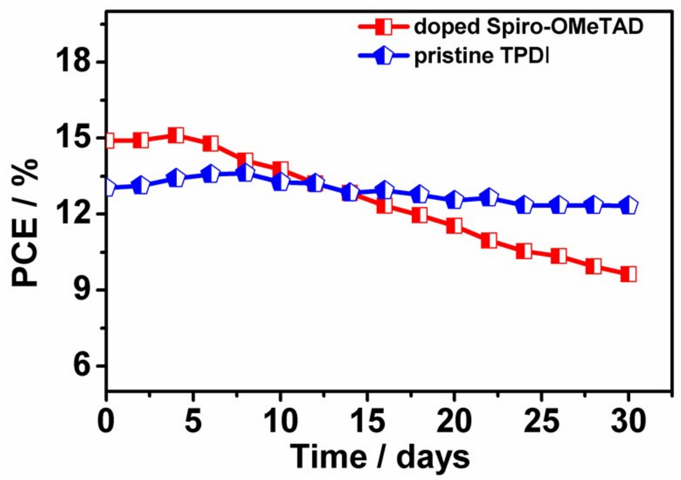

Figure S10. Time-course changes in performance of solar cells with doped spiro-OMeTAD and pristine TPDI as HTMs, respectively. The stability of the devices were monitored without encapsulation at amibient conditions (average relative humidity 42±12%, average temperature 26±5 ^{o}C), and illuminated by natural light The device performances were tested under simulated one sun illumination (~100mW.cm^{-2}) everyday.

The digital photographs on stability comparison of different HTMs–based perovskite films and the corresponding photovoltaic performance have been provided. As shown in **Figure S9** and **Figure S10**, aging under natural light at ambient atmosphere for 30 days, the $CH_3NH_3PbI_3$ / TPDI film almost kept its original dark brown color. However, the color of the $CH_3NH_3PbI_3$ / spiro-OMeTAD (doped) film gradually degraded to pale yellow of PbI_2 from the edge of the film. Moreover, the aging tests of the corresponding photovoltaic devices fabricated with different HTMs were also demonstrated. The $CH_3NH_3PbI_3$ on the surface of spiro-OMeTAD (doped) based devices presented serious degradation after 30 days in air. However, the solar cell part covered by carbon almost kept their original status of dark brown. To evaluate the effects on their photovoltaic performance, the time-course changes in efficiency of the corresponding HTM based solar cells were also recorded and shown in **Figure S10**. The TPDI-based device demonstrated apparently better stability than spiro-OMeTAD based ones. However, it is worth mentioning that the spiro-OMeTAD based devices exhibited 65% of their original efficiency even after 30 days' stability tests. This should be ascribed to the protection from carbon cathode, which acts as a water retaining layer to protect the perovskite film from being destroyed by ambient moisture. In addition, the better stability of TPDI based film and devices should also be ascribed to the good molecule stability of TPDI as being proved by thermal stability tests. Besides, the intimate contact and full coverage with the perovskite crystalline as well as its moisture resistant behavior play significant role in protecting the $CH_3NH_3PbI_3$ crystalline from being destroyed by the H_2O in the environment.